Biodiesel soot combustion: Analysis of the soot-catalyst contact in different experimental conditions

Julie Schobing, Valerie Tschamber, Alain Brillard, Gontrand Leyssens

Biodiesel soot combustion: Analysis of the soot-catalyst contact in different experimental conditions

Julie Schobing [a*], Valérie Tschamber [a], Alain Brillard [a], Gontrand Leyssens [a]

[a] Université de Haute-Alsace, LGRE (Laboratoire Gestion des Risques et Environnement) EA2334, F-68093 Mulhouse, France

***Corresponding Author. Tel: +333 89 33 61 48. E-mail: julie.schobing@uha.fr (Julie Schobing)**

Abstract

To simulate the oxidation of Biodiesel soot in a catalyzed Diesel Particulate Filter, oxidation experiments of undoped or Na-doped model soot were performed in the presence of Pt-Pd/Al_2O_3 under Temperature Programmed Oxidation and different carbon-catalyst configurations. Loose or tight contact was simulated by mixing soot and catalyst either with a spatula or in a mortar. Samples were characterized by Flame Atomic Adsorption Spectroscopy, Inductively Coupled Plasma-Optical Emission Spectroscopy, N_2-physisorption, X-ray Photoelectron Spectroscopy, Raman Spectroscopy and Transmission Electron Microscopy coupled with Energy Dispersive X-Ray. The results showed that reducing the carbon granulometry led to an enhancement of the reactivity under NO_2, due to the external combustion mechanism of carbon crystallite. In the absence of catalysts, no impact of the granulometry was observed under a flue gas containing NO and O_2. A better catalyst efficiency was obtained when the carbon-catalyst contact was increased. In tight contact, a mechanism where NO_2 can react adsorbed on a metallic site with a carbon site was proposed. In the presence of water, a simple addition of the catalytic activity of both water and Pt-Pd/Al_2O_3 catalyst impact on carbon oxidation was observed. The use of Biodiesel, simulated by Na-doped model soot, led to a significant increase in the catalyst efficiency in loose contact. Thus, a second mechanism was proposed, assuming that the doped sites play the role of NO_2-reservoir and carrier between catalyst and carbon sites.

Keywords: Biodiesel, combustion, soot-catalyst contact, catalytic oxidation

1. Introduction

These days, transportation through Diesel vehicles significantly participates in the atmospheric pollution, especially through particle emissions. According to the French Centre Interprofessionnel Technique d'Etudes de la Pollution Atmosphérique (CITEPA), the transportation sector represents around 15% of the PM_{10}, $PM_{2.5}$ and PM_1 emissions and up to 50% of the black carbon emissions in France [1]. With the aim to decrease the environmental impact of heavy-duty vehicles, Euro VI emission standards, which are mandatory since January 1st 2014, restrict particle emissions both in mass and in number [2]. The use of a Diesel Particle Filter (DPF) in the exhaust line, generally coated with a platinum (Pt) and palladium (Pd) based catalyst, is a good way to respect these standards [3]. Several authors agree that the efficiency of the catalyst is strongly affected by its contact with soot [4–12]. In order to improve knowledge on the catalytic promoting effect on soot combustion, numerous studies were conducted using model soot and catalysts. For example, Neri *et al.* [4] suggested that when a tight contact is established between graphitic carbon particles and a Pt-doped alumina catalyst, a mechanism based on a 'spillover effect' occurs. Pt is able to transfer a dissociated adsorbed oxygen atom to the soot particles with which it reacts. By monitoring DPF cross-section with an optical microscope during the loading and regeneration phases, Daido *et al.* [13] showed that the soot trapped inside the porosity of the filter are oxidized before the soot cake layer. Southward *et al.* [6] also highlighted the existence of both loose and tight contact between soot and catalyst inside a DPF. They proposed a 'de-coupling' mechanism to describe the soot combustion in the DPF. In this configuration, soot particles intimately mixed with the catalyst (i.e. inside the porosity of the filter) are oxidized by NO_2 formed on the platinum-based catalyst. On the contrary, soot particles in loose contact (i.e. distant from the washcoat) require active regeneration of the filter to be oxidized. Di Sarli *et al.* [8] observed a similar behavior with a ceria-based catalyst. They directly correlated the

amount of soot loaded in the DPF to the predominant regeneration mode of the filter (thermal or catalytic). Zhang *et al.* [14] suggested that soot-catalyst contact in real DPF conditions (in particular pressure conditions) is actually intermediate between loose and tight contact. They simulated this type of contact submitting the soot-catalyst mixture to a pressure a 60 bar in a pneumatic press. Under this more realistic contact, the oxidation of model and real Biodiesel soot in the presence of a MnO_x-CeO_2 catalyst, presented reactivity lying between the loose and tight configurations.

Reducing the carbon footprint of transport also means reducing the fossil fuel consumption as encouraged by European Directives [15]. In this context, data showed that replacing conventional Diesel fuel with Biodiesel reduces soot emission [16–19] and that Biodiesel soot appears to be more reactive [19–25], but the literature suffers from a lack of information concerning the impact of a massive use of Biodiesel on the whole depollution system line. In fact, Biodiesel, obtained by transformation of animal fats or vegetable oils, presents larger oxygen content than Diesel [16] and contains inorganic elements, such as sodium (Na), potassium (K), magnesium (Mg), calcium (Ca) or phosphorus (P). These elements could modify the composition of the soot emitted and the efficiency of after-treatment systems [25–28], although the cumulated concentrations of K + Na and Ca + Mg are limited at 5 ppm and the P content at 4 ppm by the EN 14214 standards in Europe and by the ASTM D6751 in America [29,30]. Over the lifetime and mileage of a heavy-duty truck, these inorganic impurities can significantly deposit on the various pollution control blocks [24,25,31]. In our previous works [24,25,32], it was shown that the presence of alkali metals (Na and K) in both model soot (doped by wet impregnation) and real Biodiesel soot led to an increase in their kinetic of oxidation. The beneficial impact of these inorganic elements was observed on both C-NO_2 and C-O_2 reactions. These results are supported by other authors studying various carbon materials doped with alkaline mineral and tested under O_2 and NO_2+O_2 effluent [33–

35] and real Biodiesel soot [22]. Yamane *et al.* [36] studied the filtration efficiency of a non-catalytic DPF on soot emitted from a CH_3OK-doped Biodiesel. They observed that CH_3OK is trapped in the DPF and then acts like a catalyst on soot oxidation leading to a "self-regeneration" of the filter. The catalytic soot oxidation in the presence of alkali metals within the catalyst is well documented and authors agree that these elements enhance the catalytic carbon oxidation [22,33–35,37–44]. Tikhomirov *et al.* [37] and Zhu and Wang [42] studied the impact of a KNO_3 doping of cerium based catalyst. They both attributed the higher reactivity of K-doped catalyst to the melting of KNO_3 salts on the surface, thus increasing the contact between carbon and active catalytic sites. For Gross *et al.* [40], potassium improves the catalytic activity of CeO_2 by its high mobility, generating a better contact between soot and catalyst, while Aneggi *et al.* [41] proposed that the presence of alkali metals favors the formation of carbonates acting like O-donors for the oxidation of carbon.

On the contrary, only few studies relate the impact of alkali metals on the catalytic oxidation of soot when these metals are present in the soot [35]. In their study, Zhang *et al.* [35] performed the oxidation of K- and Na-doped B7 soot by wet impregnation in the presence of a MnO_x-CeO_2 catalyst and confirmed the catalytic effect of alkali metals on carbon oxidation. However, in the case of heavy-duty trucks, catalysts currently present into DPF generally contain noble metals such as platinum and palladium. The present study aims to simulate the oxidation of Biodiesel soot in a catalyzed DPF currently used for the reduction of the particle emissions of heavy-duty trucks. In this way, the oxidation of undoped and Na-doped model soot in the presence or not of a Pt-Pd/Al_2O_3 catalysts under Temperature Programmed Oxidation (TPO) and in several flue gas (NO_2+O_2, NO_2+O_2+H_2O, NO+O_2, NO+O_2+H_2O and O_2) is performed. The impact of the contact (tight or loose) between the catalyst and soot on the oxidation of soot is investigated, considering different experimental configurations. Samples are characterized by Flame Atomic Adsorption Spectroscopy (FAAS), Inductively

Coupled Plasma-Optical Emission Spectroscopy (ICP-OES), N_2-physisorption, X-ray Photoelectron Spectroscopy (XPS), Raman Spectroscopy and Transmission Electron Microscopy (TEM) coupled with Energy Dispersive X-Ray (EDX).

2. Experimental conditions

2.1Materials preparation

2.1.1 Model Soot

Diesel soot behavior was simulated using model soot (Carbon Black Vulcan 6) denoted as CB. The model soot was doped with 0.5 wt% of sodium and is referred as CBNa in the following. Wet impregnation method with $NaNO_3$ precursor followed by a calcination step under air at 350 °C as described in [32] were used. The concentration of 0.5 wt% is attended to be representative of the one measured in real Biodiesel soot [24,32].

A Na-free CB, noted CBC (for Carbon Black – Calcined), is taken as reference. Only the calcination step at 350 °C of the impregnation protocol described in [32] was performed on this sample.

2.1.2 DPF catalyst

A Pt-Pd/Al_2O_3 catalyst composed of 0.7 wt% of platinum and 0.3 wt% of palladium supported on La-stabilized alumina was prepared by successive wet impregnations. The alumina powder (Solvay) was first compacted, ground and sieved at the 250–355 µm granulometric fraction. $Pd(NH_3)_4(NO_3)_2$ (Sigma Aldrich) was diluted in distilled water and alumina was added under agitation. The water was removed by heating at 50 °C and the powder was dried in an oven at 70 °C for 24 h. This impregnation step was then repeated with $Pt(NO_3)_2$ (Sigma Aldrich). The sample was calcined in a fixed bed reactor under synthetic air at 500 °C for 2 h. Finally, the

Pt-Pd/Al_2O_3 catalyst was stabilized in a fixed bed reactor under 10 vol.% of water in synthetic air at 650 °C for 8 h. To control the catalyst granulometry, the powder was once again compacted, ground and sieved at 250–355 µm.

2.2 Soot oxidation

2.2.1 Catalyst-Soot configurations

To evaluate the impact of the contact between carbon and catalyst on the soot oxidation, several soot-catalyst configurations with different levels of closeness between the two compounds may be tested. In the present study, the following configurations, summarized in Table 1, were tested:

- Model soot and catalyst were used either raw or manually ground in a mortar in order to modify the surface of the contact.
- Loose or tight contact was simulated by mixing soot and catalyst either with a spatula or in a mortar.
- The soot-catalyst mixture was either placed on a silica bed (Fig. 1, left), or diluted in the silica (Fig. 1 right).

Figure 1

Among the sixteen possible configurations, four are presented in the present study, as they highlight the impact of the soot-catalyst contact and of the presence of sodium on the soot reactivity. Table 1 describes the four configurations tested. Oxidation experiments (non-catalytic oxidation of soot) were also carried out on a catalyst-free to be used as reference. The model soot, raw or ground, was diluted in 200 mg of SiO_2.

Table 1

2.2.2 Reactivity test

Soot reactivity was evaluated performing Temperature Programmed Oxidation (TPO) tests in a fixed-bed reactor as described in [32]. The continuous monitoring of the temperature and outlet gases (NO, NO_2, CO and CO_2) were performed respectively by a thermocouple (K-type) located within the catalyst bed and by an infrared Rosemount Xstream analyzer. The carbon specific oxidation rate, noted V_{spe}, is expressed as:

$$V_{spe} = \frac{\left(X_{CO} + X_{CO_2}\right) * D * M_C}{10^6 * 3600 * V_M * m_{C_{ini}}}$$

where V_{spe} is expressed per gram of carbon initially introduced in the reactor ($m_{c\ ini}$), D corresponds to the flow rate in Nl/h, V_M is the molar volume (V_M = 22.4 L/mol,. X_{CO} and X_{CO2} represent the outlet concentration of, CO and CO_2 in ppmv, respectively, and M_C is the molar mass of carbon (M_C = 12 g/mol).

Table 2 gathers the five gaseous conditions considered in the present study, simulating either passive or active regeneration conditions of Diesel Particulate Filters. The case of an upstream deficient Diesel Oxidation Catalyst (no conversion of NO into NO_2 by the DOC) was also evaluated as well as the presence of water.

Table 2

2.3 Characterizations

The model soot (CB and CBNa) were fully characterized in a previous work by ultimate analyses (CHONS - Carbon, Hydrogen, Oxygen, Nitrogen, Sulfur), Flame Atomic Adsorption Spectroscopy (FAAS), Inductively Coupled Plasma-Optical Emission Spectroscopy (ICP-OES), N_2-physisorption, X-ray Photoelectron Spectroscopy (XPS) and Raman Spectroscopy [32].

182 The specific surface area of the catalyst was evaluated on a Micromeritics ASAP2020 device
183 by N_2 adsorption-desorption isotherms and calculated with the Brunauer, Emmett and Teller
184 (BET) method. The microporous contribution in the specific surface area was calculated using
185 the t-plot method. Pore size distributions were calculated on the desorption branch of the
186 isotherm by the BJH (Barrett-Joyner-Halenda) method. In the case of the carbonaceous
187 sample (microporous sample with slit pore), the Horvath-Kawazoe method was used.
188 The Pt and Pd dispersion on the surface of the catalyst was analyzed by Transmission
189 Electron Microscopy (TEM), using a JEOL ARM-200 CFEG apparatus equipped with a LaB_6
190 filament. Before analyses, samples were dispersed in chloroform and few drops of the
191 solution were deposited on a copper grid covered by a thin carbon film (5 nm). TEM
192 observations were coupled with Energy Dispersive X-Ray analysis (EDX) to determine the
193 elementary composition of the sample. TEM analyses were also performed on carbonaceous
194 sample to evaluate the size of the carbon crystallite.
195

196 # 3. Results

197 ## 3.1 Material characterizations

198 As mentioned in section 2.3., the model soot (CB and CBNa) were characterized in a previous
199 work [32]. The elemental composition of this sample, gathered in
200 Table 3, showed that after the Na-doping procedure, CB presents slightly higher oxygen
201 content. The characterization by N_2-physisorption (Table 4) also highlighted that Na-doping
202 leads to an increase in specific surface area and microporous volume [32]. This evolution of
203 the textural properties of soot with alkali metals introduction is in agreement with those
204 observed on real soot obtained when increasing the Biodiesel content in the fuel [24].
205 Moreover, total as well as microporous surface area measured on model soot (Table 4)

206 are quite similar to those obtained from real soot produced on engine test bench using
207 different Biodiesel blends [24]. The N_2-physisorption analyses prove that the carbonaceous
208 samples present micropores having a size close to 0.5 nm (Table 4). Unfortunately, precise
209 values could not be determined as they are close to the limit of detection of the N_2-
210 physisorption method. Raman Spectroscopy performed in a previous work [32] also showed
211 that Na-doping leads to a decrease in carbon structural order. XPS analyses showed that Na
212 seems to be present under a sulphated form (Na_2SO_x with x = 3 or 4). The reactivity of the
213 sample was evaluated under passive and active regeneration conditions by TPO experiments
214 under NO_2, NO_2+O_2 and NO+O_2+H_2O and thermogravimetric analyses (TGA) under O_2,
215 respectively. Experiments showed that Na has a beneficial impact on carbon oxidation
216 regardless the gas mixture on the whole temperature range studied (up to 700 °C). Thanks to a
217 numerical simulation, the study of the kinetics constants highlighted that the higher reactivity
218 of the Na-doped sample is linked to an increase in the number of actives sites but also to a
219 decrease in the activation energies of both C-NO_2 and C-O_2-NO_2 reactions [32].

220 ***Table 3***

221 ***Table 4***

222

223 Fig. 2 shows TEM micrographs of CBC and CBNa. The two samples present the typical
224 morphology of soot: agglomerate of particles formed by carbon spherules arranged in bunch
225 [45,46]. Spherules with a slightly smaller diameter are observed in the case of the doped
226 sample (CBNa). In fact, the average size of CBC spherules is approximately 30 nm against
227 25 nm for CBNa. Because of the superposition of agglomerate on the micrograph, it was
228 difficult to evaluate their size. According to the literature, soot spherules generally have a size
229 between 10 and 50 nm and the size of soot agglomerate is approximately equal to 100 µm
230 [45,46].

231 ***Figure 2***

232

233 A specific surface area of 181 $m^2/g_{support}$ was determined by N_2-physisoprtion for Pt-Pd/Al_2O_3
234 (Table 4). This value is in agreement with specific surface areas generally described in the
235 literature for γ-Al_2O_3 (< 250 m^2/g) [47]. Pt-Pd/Al_2O_3 exhibits a large distribution of pore
236 diameters between 50 and 700 Å with a maxima at 115 Å (Table 4).
237 Fig. 3 shows TEM micrographs of Pt-Pd/Al_2O_3 and the corresponding EDX mapping for
238 aluminum, lanthanum, platinum and palladium. Micrographs show that Pt and Pd are detected
239 on the whole alumina surface suggesting that they are homogeneously dispersed on the
240 catalyst. TEM micrographs also show the presence of larger metallic aggregates which seem
241 to be composed of an alloy of both platinum and palladium, with an average size of 30 nm.
242 For similar catalysts, the literature generally describes metallic particles with size around 20
243 nm [48,49].

244 ***Figure 3***
245

246 ## 3.2 Influence of CB-catalyst contact on soot oxidation

247 ### *3.2.1 Impact of the grinding*

248 The carbon specific oxidation rates, measured under NO+O_2 and NO_2+O_2 gas streams, of the raw
249 and ground Na-free CB samples (CBC) are shown in Fig. 4. Table 5 (lines 1, 2, 4 and 5) gathers the
250 values of the carbon specific oxidation rate V_{spe} measured at 400 °C for the different experiments. It
251 is well known that the soot reactivity (in absence of catalyst) towards NO is much lower than for
252 NO_2 [50] and that the carbon specific oxidation rate with few hundred ppm of NO in 10 vol.% O_2 in
253 the feed gas is virtually the same as with O_2 alone [51]. Hence, Fig. 4 confirms that ignition of CBC
254 under the NO+O_2 gas occurs below 400 °C and that a temperature higher than 650 °C is needed for
255 the complete oxidation of the sample. More interestingly, in these conditions, raw CBC and ground
256 CBC show a similar behavior on the whole temperature range, suggesting that the C-O_2 reaction is

not impacted by the carbon granulometry. Under NO_2+O_2, it is known that the carbon oxidation takes place at low temperatures (< 450 °C), mainly via the C-NO_2 reaction [52,53]. Fig. 4 shows that under the NO_2+O_2 gas stream the ignition of CBC samples starts at approximately 200 °C. Higher oxidation rates are measured until 550 °C in comparison to the results obtained under the $NO+O_2$ gas stream. In the presence of NO_2 in the gas flow, raw and ground CBC do not present the same behavior. Ground CBC sample has a significant higher reactivity. The maximum of oxidation rate is observed around 530 °C for the ground sample against 600 °C for the raw one. At 400 °C, grinding leads to an increase by 48% in the carbon oxidation rate (Table 5, lines 1 and 2). Thus, conversely to C-O_2 reaction, the C-NO_2 reaction seems to be sensitive to the carbon granulometry.

Figure 4

Table 5

3.2.2 Impact of the carbon-catalyst contact

<u>Oxidation under $NO+O_2$</u>

The oxidation of CBC in the presence of the catalyst in the four configurations and under the $NO+O_2$ gas flow is presented in Fig. 5. The carbon specific oxidation rates V_{spe} measured at 400 °C for the corresponding experiments are given in Table 5, lines 4-9.

Figure 5

Fig. 5 shows that the catalyst slightly enhances the oxidation rate of CBC, between 350 and 600 °C, when the two materials are mixed in their raw state with a spatula (RLB configuration). At 400 °C, the carbon specific oxidation rate V_{spe} is only increased by a factor 1.7 (Table 5, lines 4-9). Therefore, in this configuration, it appears that NO_2 produced by the reaction of NO and O_2 at the metallic sites does not significantly contribute to the carbon oxidation.

On the contrary, experiments carried out using the same location of the CBC-catalyst mixture in the reactor but with ground materials (GLB configuration) reveal a significant improvement in carbon oxidation rate due to the presence of the catalyst. At 400 °C, the presence of the catalyst in this

284 configuration (GLB) allows an increase in the carbon specific oxidation rate V_{spe} from
285 $2.3.10^{-2}$ mg/($s.g_{ini}$) to $7.7.10^{-2}$ mg/($s.g_{ini}$) (by a factor 3.5, Table 5, lines 5 and 7). The higher
286 reactivity of the ground catalyst, compared to the raw one, was already observed by Álvarez-Docio
287 *et al.* [11] after a mechanical activation treatment in a ball mill of a $CoAl_2O_4$ catalyst. In addition, it
288 is interesting to observe the particular shape of the TPO profile for the GLB configuration: it
289 presents a shoulder above 600 °C suggesting a two-step carbon oxidation (Fig. 5).
290 Mixing CBC and Pt-Pd/Al_2O_3 catalyst samples in a mortar (GTB configuration), to improve the
291 contact between these two materials, allows an additional increase in the oxidation rate above
292 400 °C (Fig. 5). In this configuration, the complete oxidation of carbon is achieved before 600 °C
293 (Fig. 5). The maximal oxidation rate is also significantly shifted to lower temperatures and the TPO
294 profile shows a single peak suggesting that the oxidation occurs in a one-step reaction. However,
295 despite the significant increase in the carbon oxidation rate in presence of the catalyst placed in tight
296 contact with CBC (GTB configuration), one may observe that at low temperatures (< 450 °C) the
297 obtained oxidation rate is not as high as that measured for ground CBC under the NO_2+O_2 gas flow
298 (Table 5, lines 2 and 8, and Figs. 4 and 5). Thus, it seems that Pt-Pd/Al_2O_3 is not able to oxidize all
299 the NO contained in the flue gas to NO_2. One can argue about whether the impact of the presence of
300 the catalyst in tight contact with the soot promotes the direct reaction of carbon with NO_2 and/or its
301 reaction with O_2.
302 Diluting the CBC-catalyst mixture (mixed in a mortar) into silica (GTM configuration) allows the
303 carbon oxidation rate to be even further increased. However, it can be observed that the GTB and
304 GTM configurations present very similar TPO profiles (Fig. 5). Thus the location of the CBC-
305 catalyst mixture in the reactor (on the silica bed or mixed with it) does not significantly affect the
306 carbon oxidation rate when the contact between carbon and catalyst is tight.

The study of the catalytic oxidation of CBC, under the $NO+O_2$ gaseous flow, mixed with the Pt-Pd/Al_2O_3 catalyst, showed that the soot reactivity increases according to the following order depending on the configuration: raw CBC < RLB << GLB < GTB = GTM.

Oxidation under O_2

It has been previously observed that, under the $NO+O_2$ gas flow, the contact between the soot and the catalyst greatly influences the soot reactivity above 400 °C (comparison between GLB and GTB or GTM configurations). The mechanism of O_2-spillover over platinum Al_2O_3-supported catalyst, proposed by Neri *et al.* [4], could explain the difference of reactivity observed in tight contact under $NO+O_2$. To validate this hypothesis, the oxidation of CBC in the presence of the catalyst in the GLB and GTM configurations under the feed gas composed of 10 vol.% O_2 in N_2 was performed. Fig. 6 shows that the presence of ground Pt-Pd/Al_2O_3 sample in loose contact with ground CBC (GLB configuration) leads to a slight enhancement of the carbon oxidation. A shift of the maximal oxidation rate towards lower temperatures of about fifteen degrees is observed. As no NOx is present in the feed gas, only O_2 can be used as an oxidant in these conditions. So it seems that the 'loose' contact between the catalyst and the carbon in the GLB configuration is already strong enough to favor the O_2-spillover mechanism described by Neri *et al.* [4]. When the contact between CBC and Pt-Pd/Al_2O_3 is tighter (GTM configuration), no additional improvement is observed (Fig. 6). Thus, the GTM configuration does not lead to a greater participation of the O_2-spillover mechanism in the carbon oxidation. This result leads to the conclusion that the better reactivity observed between the GTB and GLB configurations under the $NO+O_2$ gas stream (Fig. 5) is rather linked to an enhancement of the C-NO_2 reaction.

Figure 6

Influence of H_2O

Water is known for its catalytic effect on the oxidation of carbon by NO_2 [54,55]. Interactions between water, model soot and Pt-Pd/Al_2O_3 catalyst are here evaluated. Fig. 7 presents the TPO profiles obtained for the oxidation of CBC in the GTM configuration under NO_2+O_2 and NO+O_2 with and without water vapor in the flue gas. The carbon specific oxidation rates V_{spe} measured at 400 °C are given in Table 5 (lines 11-12). The specific carbon oxidation rate measured at this temperature for the non-catalytic oxidation of raw CBC under NO_2+O_2+H_2O is also reported in Table 5, line 10 (TPO profiles not shown here).

Figure 7

Whatever the initial gaseous conditions (NO_2+O_2 or NO+O_2), the addition of water leads to higher carbon oxidation rates on the whole temperature range. The complete combustion of CBC in the GTM configuration is obtained at a temperature lowered by 40 °C in the presence of water, in comparison to the dry conditions. Moreover, the beneficial impact of H_2O is identical for the two flue gas mixtures. In fact, at 400 °C, an increase in the carbon specific oxidation rate V_{spe} by 36% and 35% is observed, respectively, under NO_2+O_2 and NO+O_2 (Table 5, lines 3, 9, 11 and 12). In the case of the non-catalytic oxidation of raw CBC under NO_2+O_2, the addition of water leads to an enhancement of the same order of magnitude (increase in V_{spe} by 31% at 400 °C, Table 5, lines 1 and 10). Thus, it seems that the catalytic impact of water is not enhanced by the presence of the Pt-Pd/Al_2O_3 catalyst. These results are in agreement with the observation of Jeguirim *et al.* [56] on the isothermal oxidation of CB in the presence of a commercial Pt/Al_2O_3 catalyst.

3.3 Impact of Na-doping

To evaluate the impact of alkali metals contained in Biodiesel soot on the catalytic oxidation of carbon, the reactivity of CBNa mixed with Pt-Pd/Al_2O_3 and placed under a NO+O_2 gas stream was analyzed in the GLB and GTM configurations. The TPO profiles are presented in Fig. 8 and the specific oxidation rates V_{spe} measured at 400 °C are reported in Table 6.

Figure 8

Table 6

Contrary to CBC (Fig. 5), the presence of the catalyst in the RLB configuration with CBNa increases the specific carbon oxidation rate. In this configuration, both the maximal carbon oxidation rate and the end of the combustion of the Na-doped CB sample are shifted towards lower temperatures by about 25 °C, in comparison to the experiment carried out in absence of catalyst (Fig. 8). At 400 °C, the Pt-Pd/Al_2O_3 catalyst in loose contact with CBNa allows an increase in the specific oxidation rate V_{spe} by 8.5 (Table 6). In the CBC case, this factor was only 1.7 (Table 5, line 4 and 6). When they are present in the composition of the catalyst, alkali metals are known to enhance the catalyst activity through the improvement of the contact between the catalyst and the soot. These elements are highly mobile and are able to wet the catalyst surface (because of their low melting point) [37,40–44]. The above experiments show that the presence of 0.5 wt% of sodium on the carbon surface also improves its contact with the catalyst and thus improves the catalytic oxidation.

As observed in Fig. 8, the global impact of Pt-Pd/Al_2O_3 in tight contact (GTM configuration) has the same order of magnitude for both undoped and Na-doped CB sample under NO+O_2. The maximal oxidation rate is shifted towards lower temperatures of about 80 °C for CBNa and 90 °C for CBC. However, at low temperatures (< 450 °C), a higher impact of the catalyst is observed for the Na-doped carbon, compared to CBC. Indeed, at 400 °C in GTM configuration, the specific

oxidation rate V_{spe} is multiplied by a factor 4 with CBC, whereas this factor is equal to 25 with CBNa (by comparison with raw sample in Table 5, line 4).

4. Discussion

4.1 Impacts of the grinding and carbon granulometry

Experiments showed that decreasing the carbon granulometry has a significant impact on the carbon oxidation rate under NO_2+O_2. Under NO+O_2, grinding has only an influence in the presence of the CB-catalyst mixture. Thus it seems that the C-NO_2 reaction is particularly sensitive to the granulometry and also to the carbon surface compared to the C-O_2 reaction. This is in agreement with the work of Seong and Choi [57]. These authors characterized CB at different degrees of conversion under NO_2 or O_2 by Raman spectroscopy, Fourier Transform Infrared Spectroscopy (FTIR) and TEM. They showed that carbon oxidation by O_2 goes through an internal combustion of carbon spherules, while the oxidation by NO_2 goes through an external combustion. Moreover, the kinetic diameter of the NO_2 molecule (512 pm [58]) is very close to the size of the pore of the carbonaceous sample (close to 0.5 nm, Table 4). This is why its diffusion inside the pore of the CB is unlikely. On the contrary, O_2 molecule which shows a kinetic diameter of 346 pm is able to diffuse into the porosity of the carbonaceous sample [59]. Thus, NO_2 is sensitive to carbon granulometry, as it modifies the surface of the carbon directly in contact with the flue gas.

4.2 Impact of carbon-catalyst contact on the carbon oxidation mechanism

The results of the present study showed that the enhancement of Pt-Pd/Al_2O_3 catalytic activity is linked to an increase of the contact between carbon and catalyst and to a decrease of the

402 granulometry of the compounds. Thus, the role of Pt-Pd/Al_2O_3 regarding carbon oxidation is mostly
403 linked to the proximity between carbon sites and catalyst active sites and to the global
404 multiplication of accessible active sites to gaseous reactants.
405 When catalyst and carbon are in loose contact, it is established that carbon oxidation goes through
406 the gas phase mechanism described in Fig. 9. First, gaseous NO is oxidized in NO_2 on a metallic
407 active site. Then, NO_2 reacts with a carbon site to form CO_2 and NO. This latter could then
408 participate again to the cycle. This mechanism is highly limited by the transportation of molecules
409 in the gas phase and the probability that they meet the corresponding actives sites (represented by
410 dotted lines in Fig. 9).
411 When carbon is ground with the catalyst, a tight contact is set up suggesting that particles of the two
412 materials are closely linked (GTM and GTB configurations). Some authors highlighted an
413 O_2-spillover reaction in the case of thigh contact for platinum-based alumina-supported catalyst [4].
414 Experiments performed under a feed gas composed of 10 vol.% O_2 in N_2 showed that this
415 mechanism already occurs with the loose contact established in GLB configuration and that it is not
416 increased with a tighter contact like the one implemented in GTM and GTB configurations. Thus, it
417 can be stated that the better reactivity observed in these two last configurations is linked to an
418 improvement of the C-NO_2 reaction. An adsorption mechanism (Fig. 9) involving the adsorption
419 and the oxidation of NO into NO_2 at the carbon-catalyst interface followed by the reaction of
420 adsorbed NO_2 with carbon is proposed. The suppression of a step in the original cycle naturally
421 increases the carbon oxidation rate.
422 ***Figure 9***
423

4.3 Impact of alkali metals on the carbon oxidation mechanism

The presence of alkali metals in soot leads to an increase in the carbon oxidation rate whatever the strength of the carbon-catalyst contact. In a previous study on the reactivity of Na-, K- and P-doped carbon black, alkali metals were supposed to be able to play the role of NO_2-carrier on carbon surface through the formation of nitrates species [32]. Therefore, similarly, one may propose that NO_2 species formed by the oxidation of NO at metal sites can be adsorbed onto an alkali metal site (M) to form MNO_3 species, which then facilitate the transfer to carbon sites and thus the C-NO_2 reaction (Fig. 10). In this mechanism, a NO_2 molecule produced on a catalytic active site can be transferred to a carbon site without going into the gas phase by transportation via alkali metals sites and even if the two sites are distant (NO_2 transfer via M – Fig. 10).

Figure 10

5. Conclusion

Experiments showed that the grinding of the model soot, and thus its granulometry, has a significant impact on the C-NO_2 reaction because of the mechanism of external combustion by NO_2 of the carbon crystallite (+ 48 % of carbon oxidation rate at 400 °C under NO_2+O_2). Consequently, catalyst will have a higher impact on the oxidation of the littlest soot. When the contact between catalyst and soot increased (low granulometry or grinding in a mortar), the catalytic impact of Pt-Pd/Al_2O_3 on carbon oxidation is improved. A factor of 2.5 is retrieved between the carbon oxidation rate of the configuration with the lowest (RLB) and highest (GLB) soot-catalyst contact configuration (at 400 °C, under NO+O_2). This better efficiency is attributed to the proximity between carbon active sites and catalyst active sites, reducing the time of transportation of NO after its oxidation in NO_2. It was also proposed that, when a tight contact is established, NO_2 is able to react, being adsorbed on a metallic site,

with the carbon site without going back in the gas phase. Experiments showed that the catalytic impact of water (about + 30-35 % in carbon oxidation rate at 400 °C) cumulates with that of the catalyst. The presence of alkali metals, simulating the use of Biodiesel, led to a significant impact of catalyst efficiency. In fact, a better oxidation was observed in the simultaneous presence of Pt-Pd/Al_2O_3 and Na on the whole temperature range in loose contact. The beneficial impact of alkali metals was attributed to their capacity to wet the surface and their high mobility improving then the contact between catalyst and carbon. Thus it was proposed that alkali metals can play the role of NO_2 reservoir but also of NO_2 carrier between catalyst and carbon active sites. In addition to reducing soot production, Biodiesel is a good way to produce soot that are more reactive and are enhancing the DPF catalyst efficiency. To confirm the proposed mechanism, the influence of other parameters such as the impact of the residence time or the influence of the ramp of the TPO will be analyzed in the future.

Acknowledgment

The authors gratefully acknowledge the French National Agency for Research for its financial support (Appibio Project, Ref. ANR-14-CE22-0003).

References

[1] CITEPA. Inventaire des émissions de polluants atmosphériques et de gaz à effet de serre en France –Format Secten. 2019.
[2] Direction générale des Infrastructures, des Transports et de la Mer - Des véhicules aux normes pour réduire la pollution de l'air. 2011.
[3] Guan B, Zhan R, Lin H, Huang Z. Review of the state-of-the-art of exhaust particulate filter technology in internal combustion engines. J Environ Manage 2015;154:225–58. https://doi.org/10.1016/j.jenvman.2015.02.027.
[4] Neri G, Bonaccorsi L, Donato A, Milone C, Musolino MG, Visco AM. Catalytic combustion of diesel soot over metal oxide catalysts. Appl Catal B Environ 1997;11:217–31. https://doi.org/10.1016/S0926-3373(96)00045-8.

[5] Neeft JPA, Makkee M, Moulijn JA. Catalysts for the oxidation of soot from diesel exhaust gases. I. An exploratory study. Appl Catal B Environ 1996;8:57–78. https://doi.org/10.1016/0926-3373(95)00057-7.
[6] Southward B, Basso S. An investigation into the NO2-Decoupling of Catalyst to Soot Contact and Its Implications for Catalysed DPF Performance. SAE Int J Fuels Lubr 1(1) 2009:239–51. https://doi.org/10.4271/2008-01-0481.
[7] Issa M, Petit C, Brillard A, Brilhac J-F. Oxidation of carbon by CeO2: Effect of the contact between carbon and catalyst particles. Fuel 2008;87:740–50. https://doi.org/10.1016/j.fuel.2007.05.053.
[8] Di Sarli V, Landi G, Lisi L, Saliva A, Di Benedetto A. Catalytic diesel particulate filters with highly dispersed ceria: Effect of the soot-catalyst contact on the regeneration performance. Appl Catal B Environ 2016;197:116–24. https://doi.org/10.1016/j.apcatb.2016.01.073.
[9] Bassou B, Guilhaume N, Lombaert K, Mirodatos C, Bianchi D. Experimental Microkinetic Approach of the Catalytic Oxidation of Diesel Soot by Ceria Using Temperature-Programmed Experiments. Part 1: Impact and Evolution of the Ceria/Soot Contacts during Soot Oxidation. Energy Fuels 2010;24:4766–80. https://doi.org/10.1021/ef100581z.
[10] Piumetti M, van der Linden B, Makkee M, Miceli P, Fino D, Russo N, et al. Contact dynamics for a solid–solid reaction mediated by gas-phase oxygen: Study on the soot oxidation over ceria-based catalysts. Appl Catal B Environ 2016;199:96–107. https://doi.org/10.1016/j.apcatb.2016.06.006.
[11] Álvarez-Docio CM, Portela R, Reinosa JJ, Rubio-Marcos F, Granados-Miralles C, Pascual L, et al. Pt-free CoAl2O4 catalyst for soot combustion with NOx/O2. Appl Catal Gen 2020;591:117404. https://doi.org/10.1016/j.apcata.2019.117404.
[12] Bensaid S, Russo N, Fino D. CeO2 catalysts with fibrous morphology for soot oxidation: The importance of the soot–catalyst contact conditions. Catal Today 2013;216:57–63. https://doi.org/10.1016/j.cattod.2013.05.006.
[13] Daido S, Tagaki N. Visualization of the PM Deposition and Oxidation Behavior Inside the DPF Wall. SAE Tech Pap 2009. https://doi.org/10.4271/2009-01-1473.
[14] Zhang H, Pereira O, Legros G, Iojoiu EE, Galvez ME, Chen Y, et al. Structure-reactivity study of model and Biodiesel soot in model DPF regeneration conditions. Fuel 2019;239:373–86. https://doi.org/10.1016/j.fuel.2018.11.050.
[15] Directive 2009/28/CE du Parlement Européen et du Conseil. 2009.
[16] Agarwal AK, Gupta T, Shukla PC, Dhar A. Particulate emissions from biodiesel fuelled CI engines. Energy Convers Manag 2015;94:311–30. https://doi.org/10.1016/j.enconman.2014.12.094.
[17] Xue J, Grift TE, Hansen AC. Effect of biodiesel on engine performances and emissions. Renew Sustain Energy Rev 2011;15:1098–116. https://doi.org/10.1016/j.rser.2010.11.016.
[18] Zhang Z, Ye J, Tan D, Feng Z, Luo J, Tan Y, et al. The effects of Fe2O3 based DOC and SCR catalyst on the combustion and emission characteristics of a diesel engine fueled with biodiesel. Fuel 2021;290:120039. https://doi.org/10.1016/j.fuel.2020.120039.
[19] Du J, Su L, Zhang D, Jia C, Yuan Y. Experimental investigation into the pore structure and oxidation activity of biodiesel soot. Fuel 2022;310:122316. https://doi.org/10.1016/j.fuel.2021.122316.

[20] Song J, Alam M, Boehman AL, Kim U. Examination of the oxidation behavior of biodiesel soot. Combust Flame 2006;146:589–604. https://doi.org/10.1016/j.combustflame.2006.06.010.
[21] Lamharess N, Millet C-N, Starck L, Jeudy E, Lavy J, Da Costa P. Catalysed diesel particulate filter: Study of the reactivity of soot arising from biodiesel combustion. Catal Today 2011;176:219–24. https://doi.org/10.1016/j.cattod.2011.01.011.
[22] Löpez Suárez F-E, Bueno-López A, Illán-Gómez M-J, Ura B, Trawczynski J. Study of the uncatalyzed and catalyzed combustion of diesel and biodiesel soot. Catal Today 2011;176:182–6. https://doi.org/10.1016/j.cattod.2010.11.094.
[23] Corro G, Flores A, Pacheco-Aguirre F, Pal U, Bañuelos F, Ramirez A, et al. Biodiesel and fossil-fuel diesel soot oxidation activities of Ag/CeO2 catalyst. Fuel 2019;250:17–26. https://doi.org/10.1016/j.fuel.2019.03.043.
[24] Schobing J, Tschamber V, Brillard A, Leyssens G, Iojoiu E, Lauga V. Impact of engine operating cycle, biodiesel blends and fuel impurities on soot production and soot characteristics. Combust Flame 2018;198:1–13. https://doi.org/10.1016/j.combustflame.2018.08.025.
[25] Iojoiu E, Lauga V, Abboud J, Legros G, Bonnety J, Costa PD, et al. Biofuel Impact on Diesel Engine After-Treatment: Deactivation Mechanisms and Soot Reactivity. Emiss Control Sci Technol 2017:1–18. https://doi.org/10.1007/s40825-017-0079-x.
[26] Shukla PC, Gupta T, Labhsetwar NK, Agarwal AK. Trace metals and ions in particulates emitted by biodiesel fuelled engine. Fuel 2017;188:603–9. https://doi.org/10.1016/j.fuel.2016.10.059.
[27] Williams A, Burton J, McCornick R, Toops T. Impact of Fuel Metal Impurities on the Durability of a Light-Duty Diesel Aftertreatment System. SAE Tech Pap 2013;2013-1–513.
[28] Williams A, McCormick R, Luecke J, Brezny R, Geisselmann A, Voss K, et al. Impact of Biodiesel Impurities on the Performance and Durability of DOC, DPF and SCR Technologies. SAE Int J Fuels Lubr 2011;4:110–24. https://doi.org/10.4271/2011-01-1136.
[29] European Directives EN 14214 : 2008. n.d.
[30] American Directives ASTM D6751 n.d.
[31] Brookshear DW, Nguyen K, Toops TJ, Bunting BG, Rohr WF, Howe J. Investigation of the effects of biodiesel-based Na on emissions control components. Catal Today 2012;184:205–18. https://doi.org/10.1016/j.cattod.2011.12.001.
[32] Schobing J, Tschamber V, Brillard A, Leyssens G. Impact of biodiesel impurities on carbon oxidation in passive regeneration conditions: Influence of the alkali metals. Appl Catal B Environ 2018;226:596–607. https://doi.org/10.1016/j.apcatb.2017.12.011.
[33] Matarrese R, Castoldi L, Lietti L, Forzatti P. Soot combustion: Reactivity of alkaline and alkaline earth metal oxides in full contact with soot. Catal Today 2008;136:11–7. https://doi.org/10.1016/j.cattod.2008.03.022.
[34] Castoldi L, Matarrese R, Lietti L, Forzatti P. Intrinsic reactivity of alkaline and alkaline-earth metal oxide catalysts for oxidation of soot. Appl Catal B Environ 2009;90:278–85. https://doi.org/10.1016/j.apcatb.2009.03.022.
[35] Zhang H, He J, Li S, Iojoiu EE, Galvez ME, Xiong H, et al. Effect of Biodiesel impurities (K, Na, P) on non-catalytic and catalytic activities of Diesel soot in model DPF regeneration conditions. Fuel Process Technol 2020;199:106293. https://doi.org/10.1016/j.fuproc.2019.106293.

[36] Yamane K, Asakawa T, Numao H, Komori M. Characteristics of DPF for Diesel Engine Fueled With Biodiesel Fuel - First Report: Self-Regeneration Behavior on Vehicle Road Test and Engine Bench Rig Test. Warrendale, PA: SAE International; 2004. https://doi.org/10.4271/2004-01-1883.
[37] Tikhomirov K, Kröcher O, Wokaun A. Influence of Potassium Doping on the Activity and the Sulfur Poisoning Resistance of Soot Oxidation Catalysts. Catal Lett 2006;109:49–53. https://doi.org/10.1007/s10562-006-0055-5.
[38] Jiménez R, García X, Cellier C, Ruiz P, Gordon AL. Soot combustion with K/MgO as catalyst. Appl Catal Gen 2006;297:125–34. https://doi.org/10.1016/j.apcata.2005.08.042.
[39] Jiménez R, García X, Cellier C, Ruiz P, Gordon AL. Soot combustion with K/MgO as catalyst: II. Effect of K-precursor. Appl Catal Gen 2006;314:81–8. https://doi.org/10.1016/j.apcata.2006.08.002.
[40] Gross MS, Ulla MA, Querini CA. Catalytic oxidation of diesel soot: New characterization and kinetic evidence related to the reaction mechanism on K/CeO2 catalyst. Appl Catal Gen 2009;360:81–8. https://doi.org/10.1016/j.apcata.2009.03.011.
[41] Aneggi E, de Leitenburg C, Dolcetti G, Trovarelli A. Diesel soot combustion activity of ceria promoted with alkali metals. Catal Today 2008;136:3–10. https://doi.org/10.1016/j.cattod.2008.01.002.
[42] Zhu L, Wang X. Improving Ce0.5Zr0.5O2 soot combustion catalysts by KNO3 loading. React Kinet Mech Catal 2014;112:383–95. https://doi.org/10.1007/s11144-014-0705-3.
[43] An H, McGinn PJ. Catalytic behavior of potassium containing compounds for diesel soot combustion. Appl Catal B Environ 2006;62:46–56. https://doi.org/10.1016/j.apcatb.2005.06.013.
[44] Milt VG, Pissarello ML, Miró EE, Querini CA. Abatement of diesel-exhaust pollutants: NOx storage and soot combustion on K/La2O3 catalysts. Appl Catal B Environ 2003;41:397–414. https://doi.org/10.1016/S0926-3373(02)00175-3.
[45] Stanmore BR, Brilhac JF, Gilot P. The oxidation of soot: a review of experiments, mechanisms and models. Carbon 2001;39:2247–68. https://doi.org/10.1016/S0008-6223(01)00109-9.
[46] Xi J, Zhong B-J. Soot in Diesel Combustion Systems. Chem Eng Technol 2006;29:665–73. https://doi.org/10.1002/ceat.200600016.
[47] Trueba M, Trasatti SP. γ-Alumina as a Support for Catalysts: A Review of Fundamental Aspects. Eur J Inorg Chem 2005;2005:3393–403. https://doi.org/10.1002/ejic.200500348.
[48] Wong AP, Kyriakidou EA, Toops TJ, Regalbuto JR. The catalytic behavior of precisely synthesized Pt–Pd bimetallic catalysts for use as diesel oxidation catalysts. Catal Today 2016;267:145–56. https://doi.org/10.1016/j.cattod.2016.02.011.
[49] Graham GW, Jen H-W, Ezekoye O, Kudla RJ, Chun W, Pan XQ, et al. Effect of alloy composition on dispersion stability and catalytic activity for NO oxidation over alumina-supported Pt–Pd catalysts. Catal Lett 2007;116:1–8. https://doi.org/10.1007/s10562-007-9124-7.
[50] Stanmore BR, Tschamber V, Brilhac J-F. Oxidation of carbon by NOx, with particular reference to NO2 and N2O. Fuel 2008;87:131–46. https://doi.org/10.1016/j.fuel.2007.04.012.

[51] Setiabudi A, Makkee M, Moulijn JA. The role of NO2 and O2 in the accelerated combustion of soot in diesel exhaust gases. Appl Catal B Environ 2004;50:185–94. https://doi.org/10.1016/j.apcatb.2004.01.004.
[52] Jeguirim M, Tschamber V, Brilhac JF, Ehrburger P. Oxidation mechanism of carbon black by NO2: Effect of water vapour. Fuel 2005;84:1949–56. https://doi.org/10.1016/j.fuel.2005.03.026.
[53] Jeguirim M, Tschamber V, Brilhac JF, Ehrburger P. Interaction mechanism of NO2 with carbon black: effect of surface oxygen complexes. J Anal Appl Pyrolysis 2004;72:171–81. https://doi.org/10.1016/j.jaap.2004.03.008.
[54] Jacquot F, Logie V, Brilhac JF, Gilot P. Kinetics of the oxidation of carbon black by NO2: Influence of the presence of water and oxygen. Carbon 2002;40:335–43. https://doi.org/10.1016/S0008-6223(01)00103-8.
[55] Zouaoui N, Labaki M, Jeguirim M. Diesel soot oxidation by nitrogen dioxide, oxygen and water under engine exhaust conditions: Kinetics data related to the reaction mechanism. Comptes Rendus Chim 2014;17:672–80. https://doi.org/10.1016/j.crci.2013.09.004.
[56] Jeguirim M, Tschamber V, Brilhac JF. Kinetics of catalyzed and non-catalyzed soot oxidation with nitrogen dioxide under regeneration particle trap conditions. J Chem Technol Biotechnol 2009;84:770–6. https://doi.org/10.1002/jctb.2110.
[57] Seong H, Choi S. Oxidation-derived maturing process of soot, dependent on O2–NO2 mixtures and temperatures. Carbon 2015;93:1068–76. https://doi.org/http://dx.doi.org/10.1016/j.carbon.2015.07.008.
[58] Xie L, Liu F, Liu K, Shi X, He H. Inhibitory effect of NO2 on the selective catalytic reduction of NOx with NH3 over one-pot-synthesized Cu–SSZ-13 catalyst. Catal Sci Technol 2014;4:1104–10. https://doi.org/10.1039/C3CY00924F.
[59] Ismail AF, Khulbe KC, Matsuura T. Fundamentals of Gas Permeation Through Membranes. In: Ismail AF, Chandra Khulbe K, Matsuura T, editors. Gas Sep. Membr. Polym. Inorg., Cham: Springer International Publishing; 2015, p. 11–35. https://doi.org/10.1007/978-3-319-01095-3_2.

List of Figures

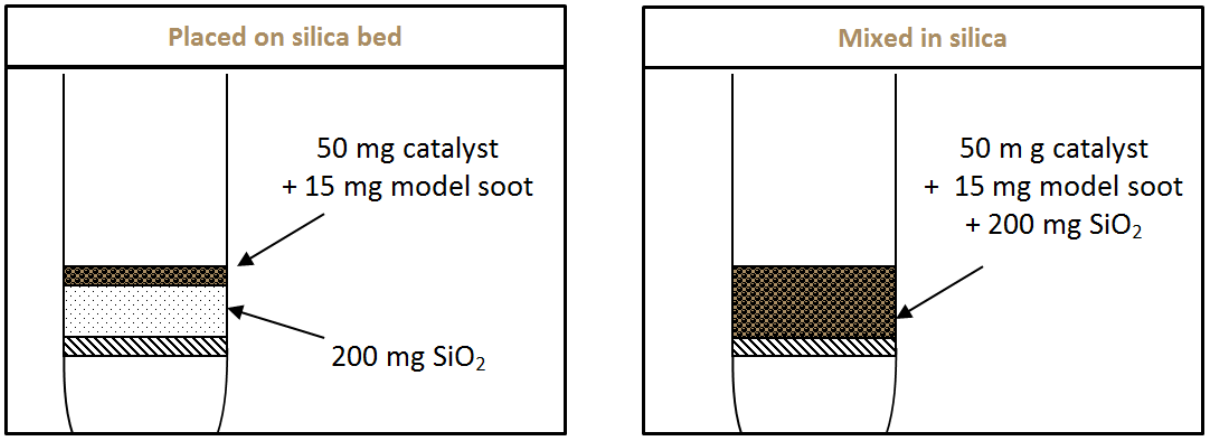

Figure 1: Schemes of the location of carbon black and catalyst mixtures in the reactor.

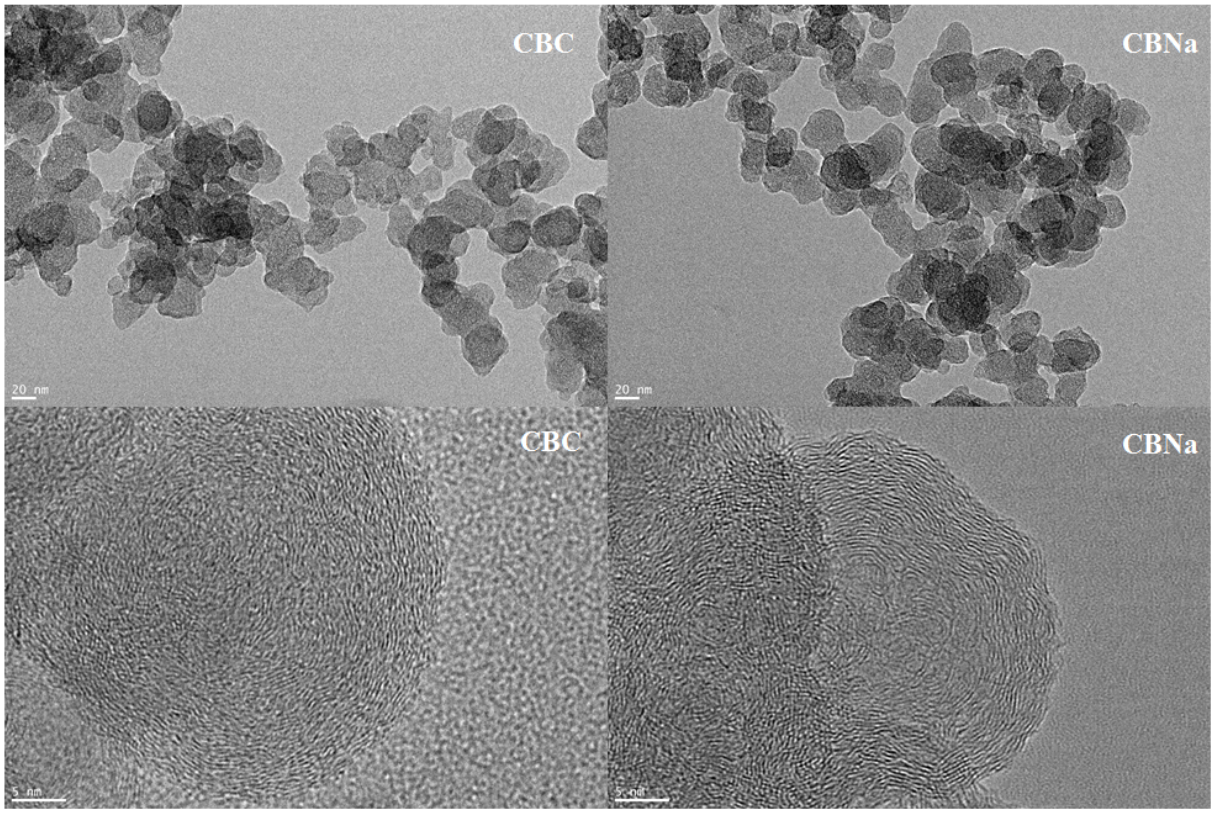

Figure 2 : TEM micrograph of CBC and CBNa

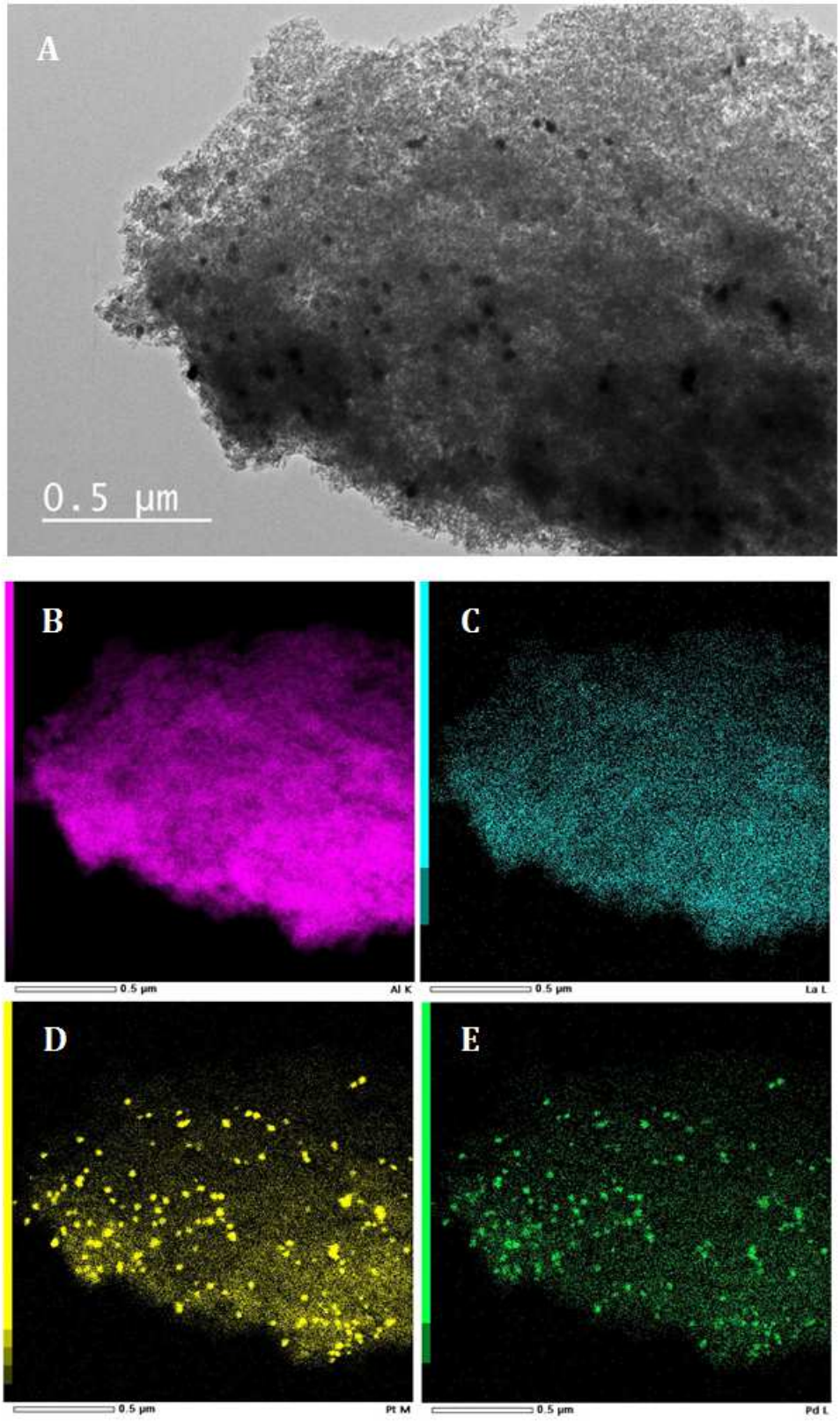

682

683 **Figure 3: TEM micrograph (A) and EDX-mapping of Pt-Pd/Al_2O_3 of, respectively,**
684 **Aluminum (B), Lanthanum (C), Platinum (D) and Palladium (E).**

685

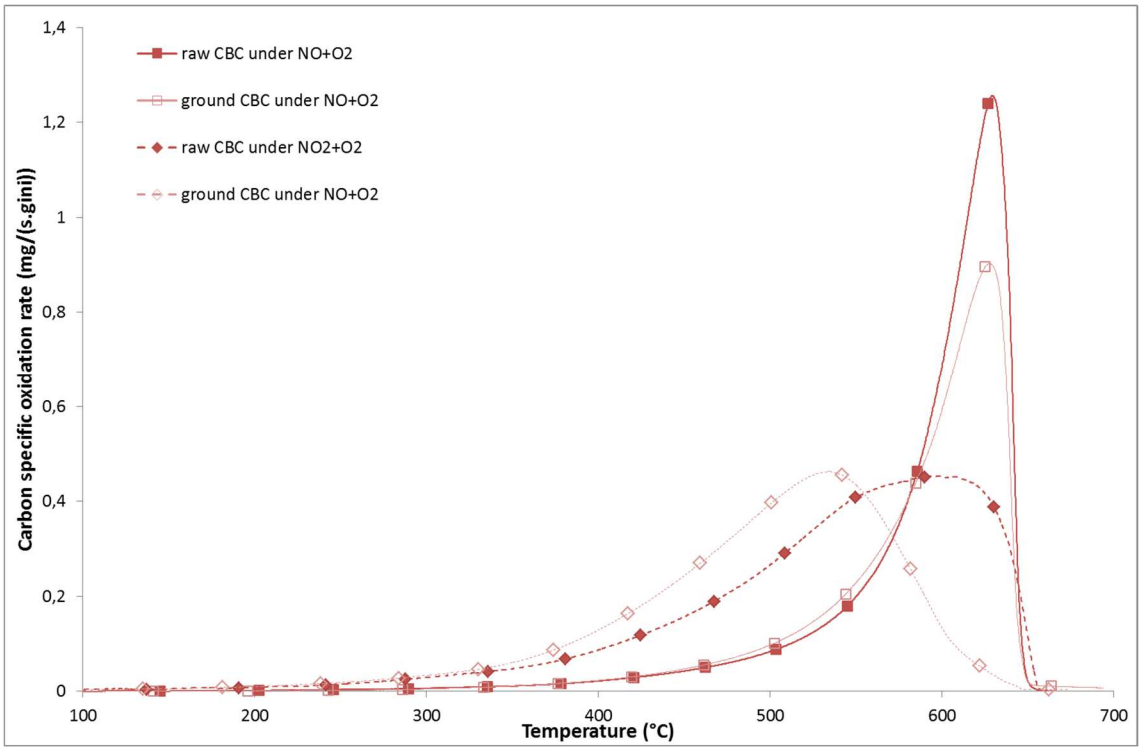

686

687 **Figure 4: Evolution of the carbon specific oxidation rate with the temperature of raw and**
688 **ground undoped black carbon under $NO+O_2$ and NO_2+O_2**

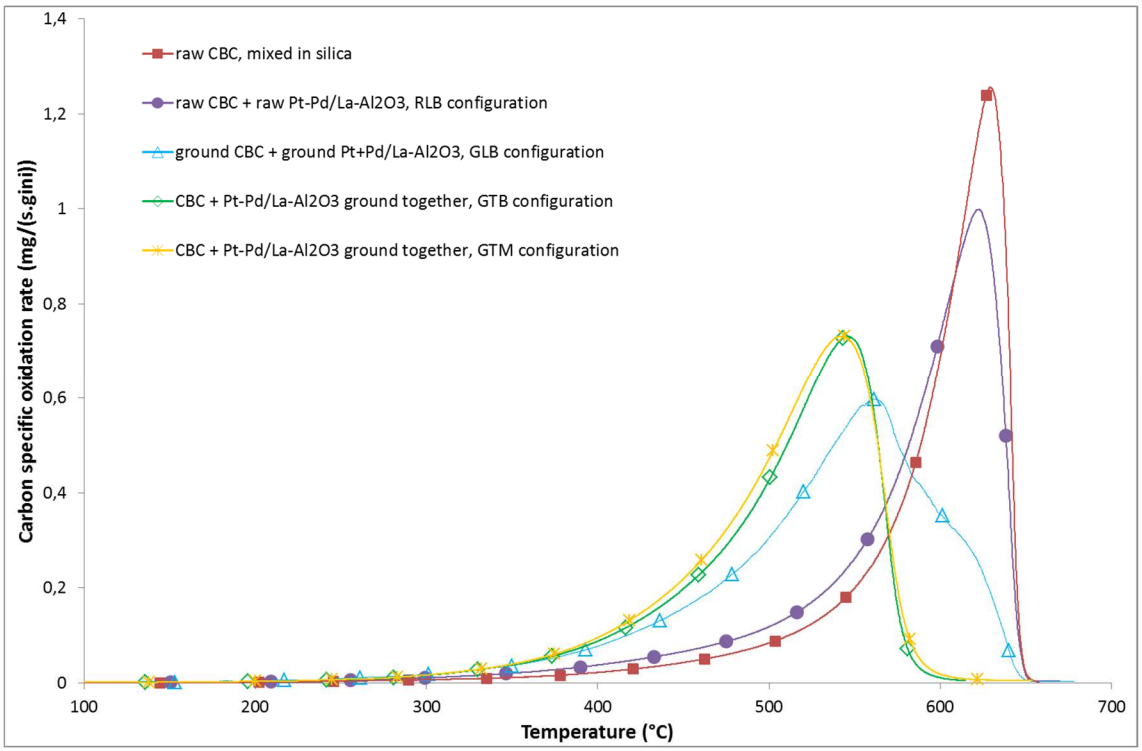

689

690 **Figure 5: Evolution of the carbon specific oxidation rate with the temperature of the**
691 **catalytic oxidation of undoped black carbon under passive regeneration conditions**
692 **($NO+O_2$) and different carbon-catalyst configurations.**

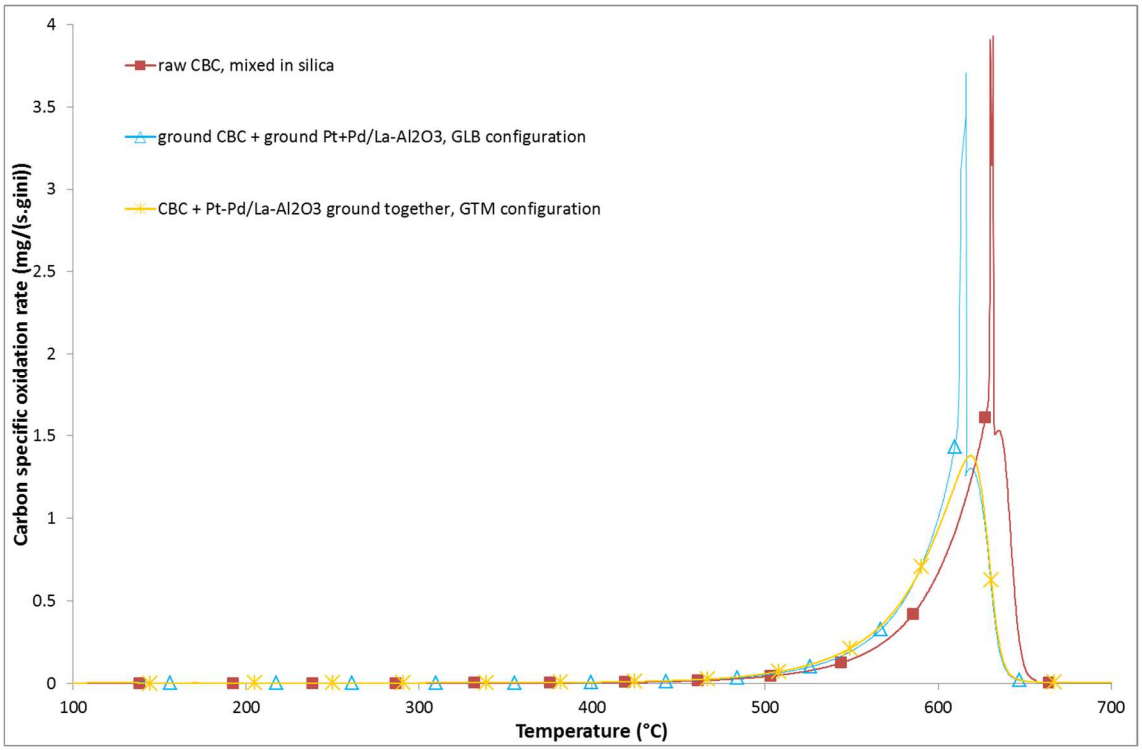

Figure 6: Evolution of the carbon specific oxidation rate with the temperature of the catalytic oxidation of undoped black carbon under active regeneration conditions (O_2) and different carbon-catalyst configurations.

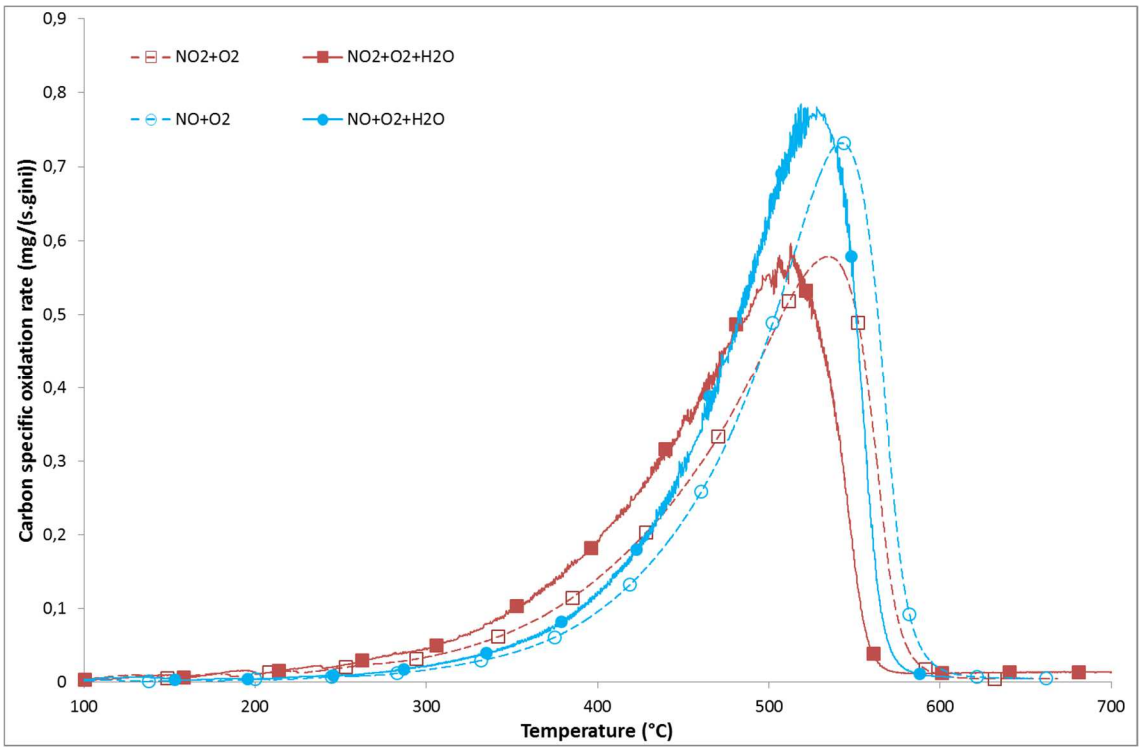

Figure 7: Evolution of the carbon specific oxidation rate with the temperature of the catalytic oxidation of undoped black carbon in GTM configurations under different flue gas containing water or not.

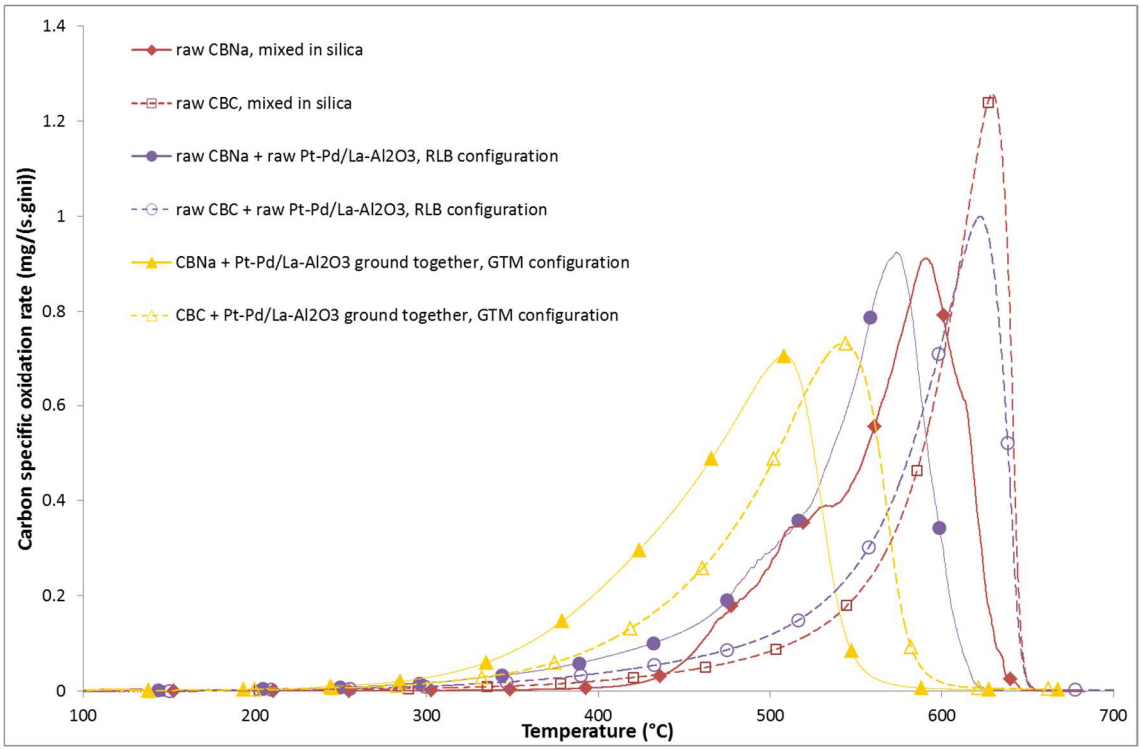

703

704 **Figure 8: Evolution of the carbon specific oxidation rate with the temperature of undoped**
705 **and Na-doped black carbon under passive regeneration conditions ($NO+O_2$) and different**
706 **carbon-catalyst configurations.**

707

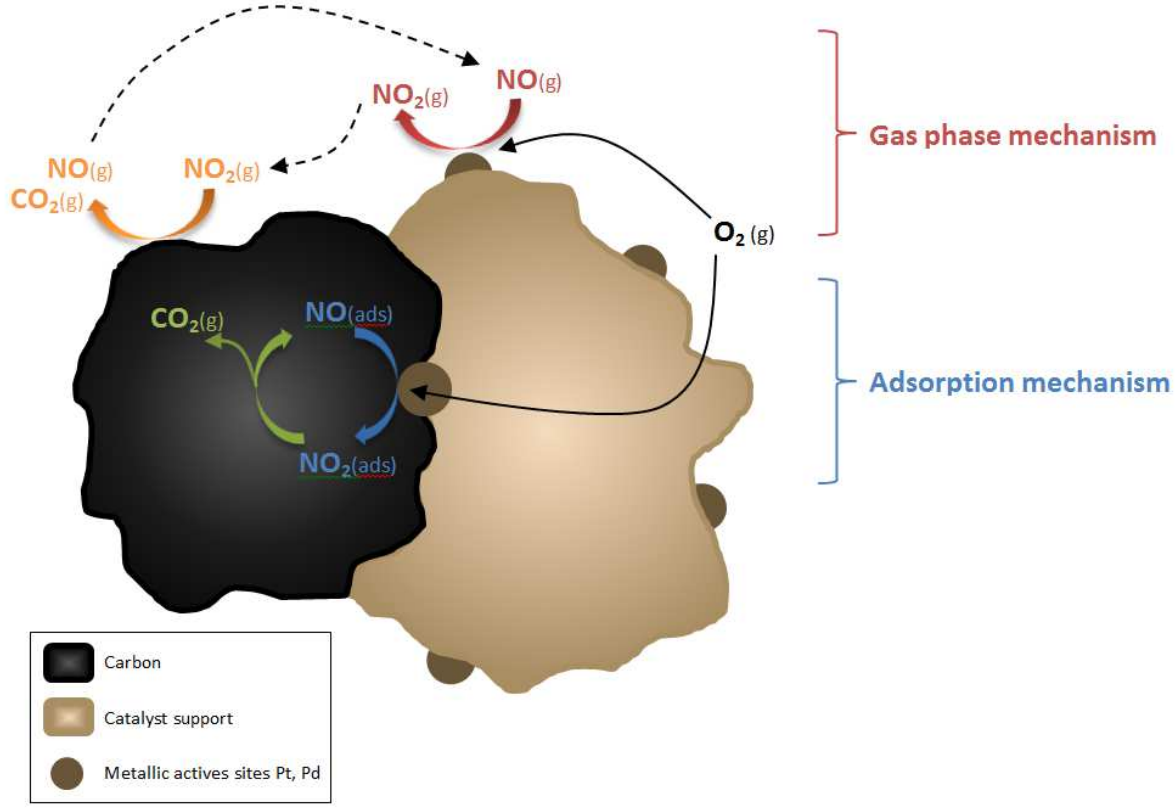

708

709 **Figure 9: Proposition of mechanism for the catalytic oxidation of carbon.**

710

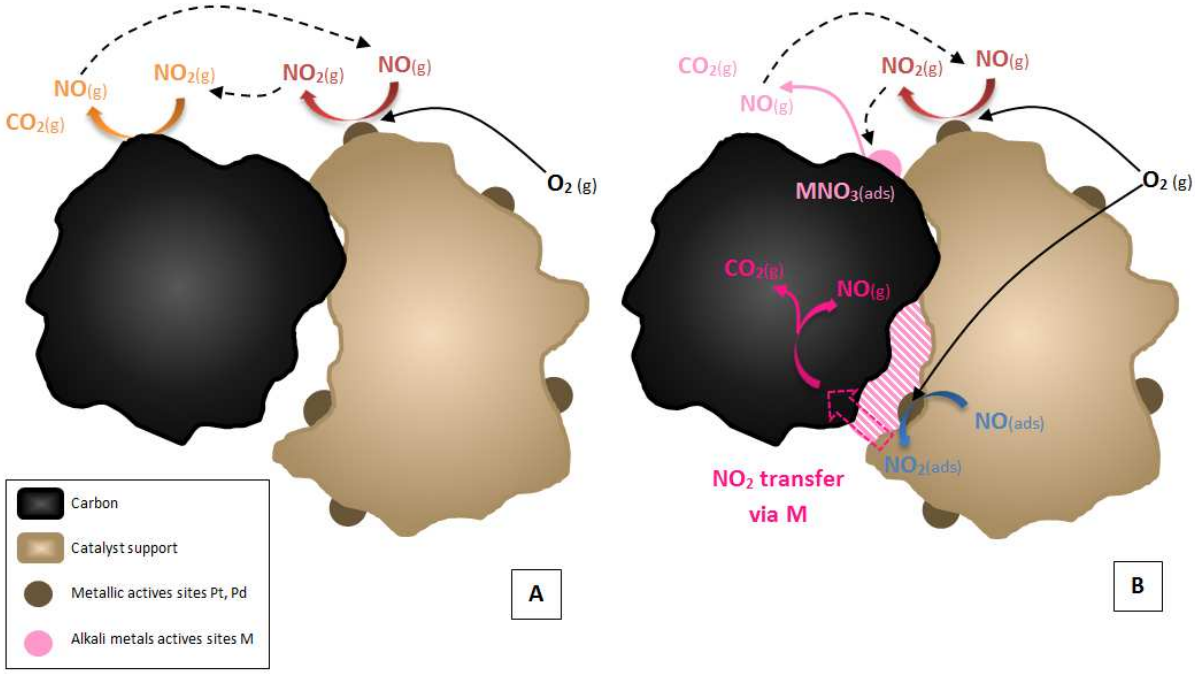

711

712 **Figure 10: Proposition of mechanism for the carbon oxidation with a catalyst in low**
713 **contact (A) with no alkali metals and (B) with alkali metals.**

714

List of Tables

Table 1: Description of soot-catalyst configurations tested in fixed bed reactor.

Configuration	Model Soot	Catalyst	Strength of contact (Mixing)	Placement
RLB	**R**aw	**R**aw	**L**oose (Spatula)	**B**ed
GLB	**G**round	**G**round	**L**oose (Spatula)	**B**ed
GTB	**G**round	**G**round	**T**ight (Mortar)	**B**ed
GTM	**G**round	**G**round	**T**ight (Mortar)	**M**ixed

Table 2: Gas composition of the conditions simulated in TPOs.

Notations	Gas concentrations in N_2				Simulated Conditions
	NO_2 (ppmv)	NO (ppmv)	O_2 (vol. %)	H_2O (vol. %)	
NO_2+O_2	400	0	10	0	Passive regeneration
$NO_2+O_2+H_2O$	400	0	10	4	
$NO+O_2$	0	400	10	0	Passive regeneration with DOC failure
$NO+O_2+H_2O$	0	400	10	4	
O_2	0	0	10	0	Active regeneration

Table 3: Elemental composition of the doped carbons black in wt% ([1]CHONS, [2]AA, [3]ICP, n.m. = not measured, n.d. = not detected).

Sample	C[1]	H[1]	O[1]	N[1]	S[1]	Na[2]	K[2]	P[3]
CBC	91.5	0.23	3.31	0.10	0.73	0.01	0.01	n.d.
CBNa	88.7	0.44	5.15	0.13	0.97	0.55	n.d.	n.m.

Table 4: Textural properties of the sample (1Horvath-Kawazoe method, 2BJH method)

Sample	Specific surface area ($m^2/g_{support}$ STP)		Average pore diameter (nm)
	Total	Microporous	
CBC	256	117	$\leq 0.6^1$
CBNa	328	218	$\leq 0.6^1$
$Pt\text{-}Pd/Al_2O_3$	181	41	11.5^2

737 **Table 5: Carbon specific oxidation rate at 400 °C of the different experiments with CBC.**

Configuration	Gas	V_{spe} at 400 °C (10^{-2} mg/(s.g_{ini}))
raw CBC	NO_2+O_2	8.7
ground CBC		12.9
GTM		14.0
raw CBC	$NO+O_2$	2.2
ground CBC		2.3
RLB		3.8
GLB		7.7
GTB		8.8
GTM		9.5
raw CBC	$NO_2+O_2+H_2O$	11.4
GTM		19.1
GTM	$NO+O_2+H_2O$	12.8

738

739 **Table 6: Carbon specific oxidation rate at 400 °C of the different experiments with CBNa.**

Configuration	Gas	V_{spe} at 400 °C (10^{-2} mg/(s.g_{ini}))
Raw CBNa	$NO+O_2$	0.8
RLB		6.8
GTM		20.1

740

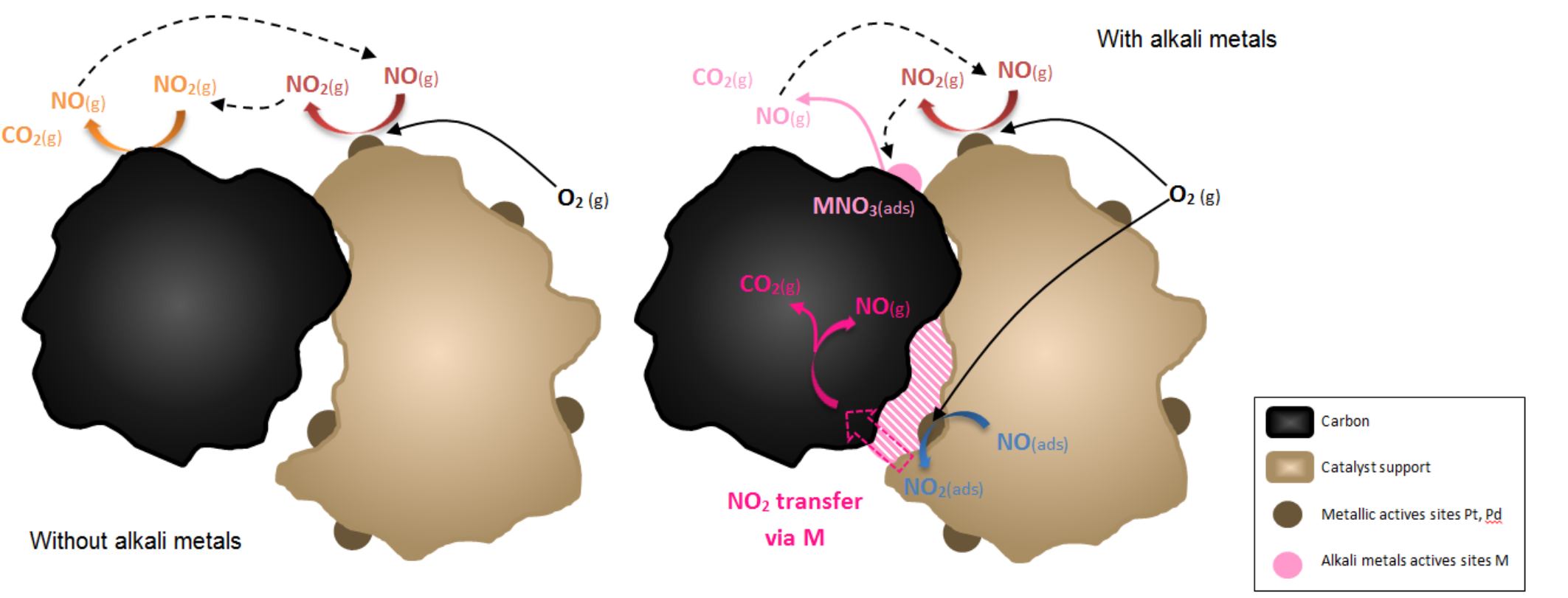
With alkali metals
NO(g)
NO2(g)
NO2(g)
NO(g)
CO2(g)
O2 (g)
Without alkali metals
CO2(g)
NO(g)
NO2(g)
NO(g)
MNO3(ads)
O2 (g)
CO2(g)
NO(g)
NO(ads)
NO2(ads)
NO2 transfer
via M
Carbon
Catalyst support
Metallic actives sites Pt, Pd
Alkali metals actives sites M